International Journal of
Science and Engineering Investigations
vol. 9, issue 102, July 2020
Received on July 13, 2020
ISSN: 2251-8843

Transitional Flow and Heat Transfer over a Backward-Facing Step with an Inserted Cylinder

S. Zou[1], J. H. Xu[2], K. Inaoka[3], G. N. Xi[4]
[1,3]Department of Mechanical Engineering, Doshisha University, Kyotanabe 610-0321, Japan
[2,4]Department of Mechanical Engineering, Nantong University, Nantong 226019, China
([1]doctorshuaizou@gmail.com)

Abstract-In this study, the forced convection characteristics of transitional fluid flow and heat transfer enhancement in a two-dimensional, backward-facing step channel by inserting an adiabatic cylinder were numerically investigated. The computational fluid dynamics simulations were performed using finite volume method in the commercial package Ansys Fluent. The effects of various streamwise positions (X_C/S = 0.6, 0.9, 1.2, and 1.5) and cross-stream positions (Y_C/S = 0.5, 1.0, and 1.5) of the cylinder were examined for a fixed diameter of the inserted cylinder (d/S = 0.4). As per the results, a 114% enhancement of the overall heat transfer on the bottom wall could be achieved by inserting an adiabatic cylinder at X_C/S = 0.6 and Y_C/S = 1.0 as compared with the case without the cylinder. Additionally, the insertion of a cylinder significantly diminishes the deterioration of heat transfer in the primary recirculation zone.

Keywords- *Computational Fluid Dynamics, Forced Convection, Transitional Flow, Heat Transfer, Backward-Facing Step, Adiabatic Cylinder*

I. INTRODUCTION

Backward-facing step flow is one of the most fundamental models to trigger a stepwise flow separation and reattachment behavior. Study of such flows has been gaining prominence due to its extensive application in energy system equipment, dump combustors, turbine blades, and heat-exchanging devices. The fluid flow over the backward-facing step has been adapted as a typical research model to achieve a comprehensive insight into these separated and reattached flows. Many detailed reviews on this subject are referenced in the literature [1-3].

Laminar and turbulent flow in a backward-facing step channel have been extensively investigated using experimental [4-7] and numerical methods [8-14]. Additionally, three-dimensional backward-facing step flow has become a popular field of study in fluid dynamics since Armaly et al. proposed the advancement of this method [4]. The laminar flow regime (Re_D <1200), transitional flow regime (1200$\leqslant Re_D \leqslant$6600), and turbulent flow regime (Re_D>6600) were identified based on primary reattachment length using laser Doppler measurements. Chiang and Sheu [15] numerically investigated the effects of spanwise width ($2h \leqslant B \leqslant 100h$) on the flow regime in the range of $100 \leqslant Re_D \leqslant 1000$. Their results obtained the two-dimensional behavior of the flow at the center plane when the spanwise width was increased to $100h$ at Re_D=800. Iwai et al. [16] investigated the heat transfer distribution on the bottom wall with the effect of the aspect ratio of the flow tunnel in the laminar flow regime ($125 \leqslant Re_S \leqslant 375$). The peak *Nu,* which was distributed close to the side walls, increased with an increase in the aspect ratio. Lan et al. [17] reported the predictions of turbulent flow over a three-dimensional backward-facing step with a new turbulent model ($\kappa-\varepsilon-\zeta$- *f*). Thus, there was a significant improvement in the accuracy of heat transfer predictions in separated or bounded flows at a high *Re* range of 20000–50000. The results showed that an increase in the *Re* and aspect ratio led to an increased bulk *Nu*.

Few studies have been conducted on the heat transfer characteristics in the transitional flow regime over a backward-facing step because of instability and complexity issues. Kaiktsis [18] used numerical simulations to study the early transition and three-dimensionality of the backward-facing step flow. Bifurcation of two-dimensional flow to three-dimensional flow was observed at Re_D=700. Schäfer et al. [19] simulated the late transitional backward-facing step flow using direct numerical simulation (DNS) and found that the oscillations of the primary recirculation zone and upper wall recirculation zone are dominated by bubble structures in the late transitional regime (Re_D=6600). Kitoh et al. [20] reported the effects of expansion ratios on the time-averaged reattachment length and improved heat transfer characteristics at an unsteady flow state using the DNS. Xu et al. [21] numerically investigated the unsteady flow over a three-dimensional backward-facing step. Periodic flow instability influences the heat transfer augmentation at the center of the bottom wall. Tihon et al. [22] experimentally studied the transitional flow (water) with variable expansion ratios at moderate Reynolds numbers. Their results suggested that the pulsatile inlet flow is essential in the flow structures, reattachment length, and upper wall recirculation zone.

Recently, researchers investigated the influence of obstacles inserted in the backward-facing step on the flow fields and heat transfer. Kumar and Dhiman [23] numerically simulated the flow and thermal fields in a backward-facing step with different cross-stream positions (y_c) of the inserted cylinder in the laminar regime ($1 \leqslant Re_S \leqslant 200$). The maximum increase in

pressure drop for y_c=1.5 at Re_S=200 was approximately 37%, whereas the maximum Nusselt number increased by approximately 155% when compared with the unobstructed case. Selimefendigil and Öztop [24] applied the system identification method to forecast the thermal property with the effects of pulsating flow over a backward-facing step using a fixed cylinder. A significant enhancement of heat transfer was observed with an increase in Reynolds number, pulsation frequency, and nanoparticle volume fraction. Further, they numerically investigated the effects of the pulsating flow on the heat transfer in a backward-facing step equipped with an adiabatic thin fin. The adiabatic thin fin was not effective for heat transfer. Mohammed et al. [25] simulated a convective nanofluid flow in a backward-facing step with baffles combining laminar and turbulent flows. The locations, distance, and height of the baffles were observed to significantly influence the heat transfer rather than the number and width of the baffles. Selimefendigil and Öztop [26] used a backward-facing step with a corrugated bottom wall in a forced convection nanofluid in their study of heat transfer characteristics. The results showed that the height and length of the corrugation wave influenced the heat transfer enhancement.

The analysis and study of transitional forced convection flow and heat transfer over a backward-facing step by inserting a cylinder is unexplored. Thus, the primary objective of this study is to transform the laminar flow into a transitional flow in a backward-facing step channel using an inserted cylinder. Further, we investigated the effects of various streamwise and cross-stream positions of the cylinder on the flow fields and heat transfer enhancement using computational fluid dynamics (CFD) simulations. We describe the heat transfer mechanism in a transitional backward-facing step flow in the presence of an inserted cylinder.

II. NUMERICAL METHODOLOGY

A. Problem Description and Mathematical Formulation

A schematic of the computational domain is presented in Fig. 1. The step height S is the non-dimensional length scale. The upstream of the duct height (h) and channel height downstream from step (H) are maintained constant throughout this study. The duct expansion ratio, $ER=H/h$, was set to two. The channel lengths, upstream and downstream, of the step are L_u (L_u=1S) and L_d (L_d=60S), respectively.

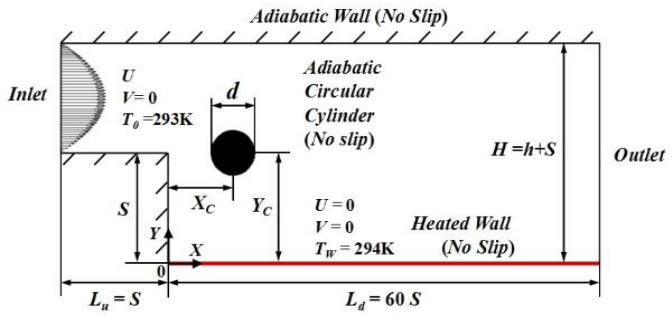

Figure 1. Schematic of the computational domain.

The upstream flow before the step was set at X/S=-1 to avoid the influence caused by the sudden expansion at the step. The position corresponding to X/S=60 following the step is set as the boundary of the calculation region in the model in Ansys Fluent, whereas, the fore part of the flow is the research region in the present study, so as to avoid the influence of outflow. The upstream inlet flow is laminar, fully developed, and isothermal (T_0=293 K). The downstream bottom wall of the backward-facing step is maintained at a uniform temperature (T_W=294 K). The buoyancy effect is negligible because the above inlet flow and bottom wall share similar temperatures. The remaining walls, including the cylinder wall, were treated as adiabatic. A high heat transfer coefficient is attained at the reattachment point, and the primary recirculation zone exhibits an inferior heat transfer property. An adiabatic cylinder is mounted near the top corner in the backward-facing step channel to create disturbances and improve the deteriorated heat transfer in the primary recirculation zone. Various streamwise positions (X_C/S=0.6, 0.9, 1.2, and 1.5) and cross-stream positions (Y_C/S=0.5, 1.0, and 1.5) of the cylinder were investigated with a fixed cylinder size (d/S=0.4).

For the two-dimensional, laminar, incompressible, and unsteady case, the governing equations are: continuity (1), momentum equations in the *x*- and *y-directions* (2) and (3), respectively, and energy equations (4).

$$\rho\frac{\partial U}{\partial X}+\rho\frac{\partial V}{\partial Y}=0 \tag{1}$$

$$\rho\frac{\partial U}{\partial t}+\rho\frac{\partial U^2}{\partial X}+\rho\frac{\partial VU}{\partial Y}=-\frac{\partial P}{\partial X}+\mu\left(\frac{\partial^2 U}{\partial X^2}+\frac{\partial^2 U}{\partial Y^2}\right) \tag{2}$$

$$\rho\frac{\partial V}{\partial t}+\rho\frac{\partial UV}{\partial X}+\rho\frac{\partial V^2}{\partial Y}=-\frac{\partial P}{\partial Y}+\mu\left(\frac{\partial^2 V}{\partial X^2}+\frac{\partial^2 V}{\partial Y^2}\right) \tag{3}$$

$$\rho\frac{\partial T}{\partial t}+\rho\frac{\partial UT}{\partial X}+\rho\frac{\partial VT}{\partial Y}=\frac{k}{C_P}\left(\frac{\partial^2 T}{\partial X^2}+\frac{\partial^2 T}{\partial Y^2}\right) \tag{4}$$

where U and V represent the two instantaneous components of the velocity; T, P, and t represent the temperature, pressure, and time, respectively; and ρ, μ, C_p, and k represent the density, dynamic viscosity, specific heat, and thermal conductivity, respectively. The physical properties of the fluid (air) are assumed to be constants. In the energy equation, the viscous dissipation is assumed to be negligible**.**

The boundary conditions in the non-dimensional form are written as follows:

- At the inlet, the streamwise velocity component is assumed according to the velocity approximation proposed by Shah and London [27] and the inlet temperature is uniform,

$$\left(U=\frac{3}{2}U_0\left[1-\left(\frac{(Y-S)-(H-S)/2}{(H-S)/2}\right)^2\right],\ V=0 \text{ and } T_0=293 \text{ K}\right).$$

- At the outlet, the outflow boundary condition is assumed to be fully developed, and the stream-wise gradient of flow variables is zero, ($\frac{\partial U}{\partial X}=0$, $\frac{\partial V}{\partial X}=0$ and $\frac{\partial T}{\partial X}=0$).

- All walls meet the no-slip condition ($U = 0$, and $V = 0$). The bottom wall was heated at a uniform temperature (T_W = 294 K). The other walls were considered adiabatic.

The local Nusselt number, time-averaged Nusselt number, and time-spatial averaged Nusselt number are defined as:

$$\mathrm{Nu}=\frac{q_W S}{k(T_W-T_0)} \tag{5}$$

$$\overline{\mathrm{Nu}}_t=\frac{1}{\tau}\int_0^{\tau}\mathrm{Nu}\ \mathrm{dt} \tag{6}$$

$$\overline{\mathrm{Nu}}=\frac{1}{L}\int_0^{L}\overline{\mathrm{Nu}_t}\ \mathrm{dX} \tag{7}$$

where q_W represents the wall heat flux, k is the thermal conductivity of the fluid, τ is the total time of ten cycles, and L is the streamwise length of the bottom wall.

The total pressure drop coefficient and Reynolds number are given by

$$\mathrm{dP}=\frac{2(\overline{P_0}-\overline{P_{out}})}{\rho U_0^2} \tag{8}$$

$$\mathrm{Re}=\mathrm{Re_S}=\frac{\rho U_0 S}{\mu},\quad \mathrm{Re_D}=2\,\mathrm{Re_S} \tag{9}$$

where is $\overline{P_0}$ the average inlet pressure and $\overline{P_{out}}$ is the average outlet pressure. U_0 denotes the averaged velocity of the inlet flow and S is the reference length.

B. Numerical Solution Procedure

The numerical study was conducted using the commercial package Ansys Fluent v18.0 (Ansys Inc., PA, USA). The finite volume method is used for the spatial discretization of (1)–(4). The convective terms in the Navier–Stokes equations and energy equations are evaluated using the QUICK scheme. The SIMPLE algorithm proposed by Patankar and Spalding [28] is utilized for the coupling of pressure and velocity. The initial conditions of the velocity components and temperature were set as U=U_0, V=0, and T_0=293 K. The grid was generated using the preprocessing tool Ansys ICEM CFD. In (10), the time increment (Δt) between two successive time steps is set to maintain the Courant number (c) to less than 1 and evaluated with the smallest grid spacing (ΔX_{min}) and maximum velocity ($U_{\max}$=1.5U_0).

$$c=\frac{U_{\max}}{\Delta X_{\min}}\leq 1 \tag{10}$$

C. Grid Testing and Validation Study

Fig. 2(a) shows a magnified view of the non-uniform grid structure for an unobstructed case. Grid refinement was performed in the regions around the walls, where the velocity gradient was high. Similarly, the magnified view of the grid structure with a cylinder is shown in Fig. 2(b). To capture the flow information around the cylinder, a fine grid is established in a square region. The density of the grid is essential in the calculation results. The numerical calculation accuracy is reduced with a coarse grid, resulting in a deviation from the true solution. Contrarily, the very fine grid consumes much more memory and CPU time. Thus, an optimal grid design is essential for balancing calculation accuracy and time consumption.

The grid Reynolds number (Re_g), which defines the minimum grid spacing (ΔX_{min}) as the reference length, can reflect the grid density. It is expressed as:

$$\mathrm{Re_g}=\frac{\rho U_0 \Delta X_{\min}}{\mu} \tag{11}$$

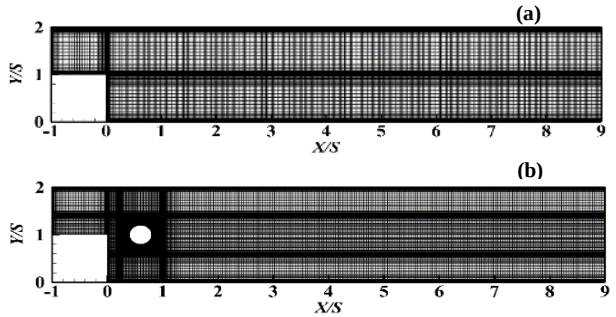

Figure 2. Magnified views of the grid: (a) no cylinder and (b) with a cylinder.

Table 1 shows that the grid independence study was conducted with three different types of grid sizes when Y_C=1.0. The deviation was calculated based on the data for Re_g=4. As Re_g decreases, the deviation of these values becomes smaller. When Re_g=8, the minimum deviation is approximately -0.11%, while the maximum deviation is approximately -1.88%, thus meeting the requirement of grid independence. Consequently, Re_g=8 is the value set in these simulations.

The validation of streamwise velocity profiles when Re=500 is presented in Fig. 3. A flow behavior similar to that observed in the study by Cuerrero and Cotta [29] can be observed and is consistent with our results. For comparison, our result corresponding to the reattachment length at Re=700 is shown in Table 2 with previously reported values [4, 5, 30].

The minimum deviation when compared with the experimental results (ER=2) of the study by Lee and Mateescu [5] is 1.30%, while the maximum deviation is -6.14% when compared with that (ER=1.94) in the study by Armaly et al. [4]. Additionally, the relatively small deviation when compared with the numerical results (ER=2) of the study by Sugarawara et al. [30] is -2.32%. In the presence of a cylinder, the time-averaged Nusselt number when compared with the numerical results of the study by Kumar and Dhiman [23] when Y_C/S=1.0 and Re=200 is presented in Fig. 4. The maximum deviation at the peak value was -4.48%. Thus, the reliability and accuracy of our numerical solution procedure can be confirmed.

TABLE I. GRID INDEPENDENCE STUDY

Re_g	Grid size	X_R/S	Dev. (%)	$\overline{Nu_{tmax}}$	Dev. (%)	$\overline{Nu}$	Dev. (%)
16	84,138	0.901	-1.42	13.574	4.73	3.373	-5.57
8	152,898	0.913	-0.11	12.985	0.19	3.505	-1.88
4	209,228	0.914	0.00	12.961	0.00	3.572	0.00

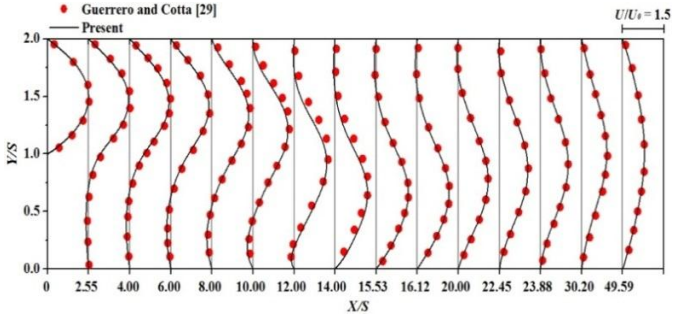

Figure 3. Comparison of streamwise velocity profiles for *Re* = 500.

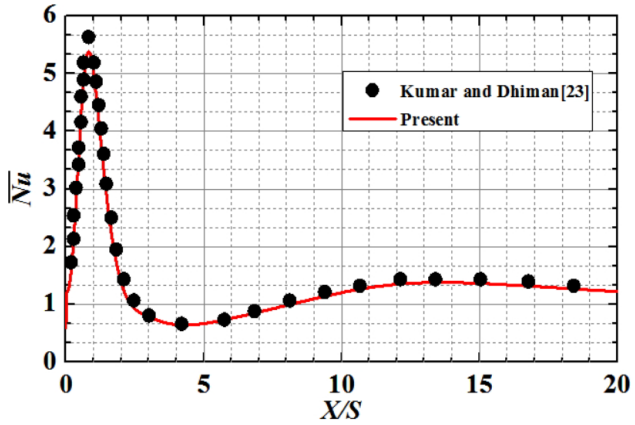

Figure 4. Comparison of the time-averaged Nusselt number distribution.

TABLE II. REPORTED VALUES FOR THE TIME-AVERAGED REATTACHMENT LENGTH X_R/S AT RE = 700

Source	X_R/S	Dev. (%)
Present	14.66	0.00
Armaly et al. [4]	13.76	-6.14
Lee and Mateescu [5]	14.85	1.30
Sugarawara et al. [30]	14.32	-2.32

III. RESULTS AND DISCUSSION

A. *Effect of Cross-stream Position*

Fig. 5 presents the flow patterns with the effect of the cross-stream position of the cylinder (Y_C/S=0.5, 1.0, and 1.5) at *Re*=700. Without a cylinder, a steady laminar flow can be observed. The primary recirculation zone appears adjacent to the step with a reattachment length of 14.6. The secondary recirculation zone could be detected downstream near the upper wall. The two recirculation zones after inserting a cylinder at Y_C/S=0.5 share the same structural properties as that of the no cylinder case. Considering the low reverse velocity inside the primary recirculation zone behind the step, the position at Y_C/S=0.5 of the cylinder is not effective for forced convection. The flow state experienced a significant mutation and emerged as a newly formed transitional flow regime at Y_C/S=1.0 and 1.5. Thus, the primary recirculation zone would be broken owing to the divided shear layer, primarily due to the presence of the cylinder. A series of vortices appear near the bottom wall when Y_C/S=1.0. Further, a vortex could be observed near the upper wall. As the position of the cylinder moved to the center of the inlet entrance, the vortex street near the bottom wall disappeared, and the number of vortices near the upper wall increased with reduced sizes.

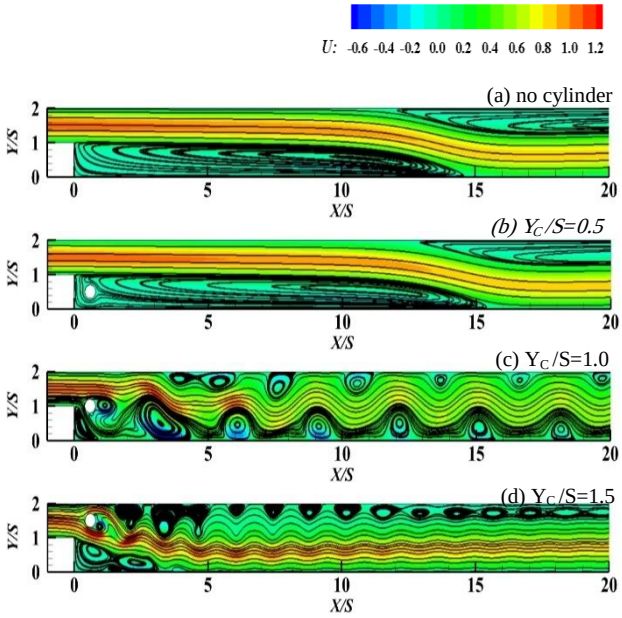

Figure 5. Instantaneous streamlines and streamwise velocity contours with various cross-stream positions for *Re* = 700.

To investigate the effect of the cross-stream position on the heat transfer characteristics, the time-averaged Nusselt number distributions on the bottom wall for all cases at *Re*=700 are illustrated in Fig. 6. Owing to the similar flow structure for the case with no cylinder and Y_C/S=0.5, the curve of the time-averaged Nusselt number on the bottom wall has a similar shape. When the cylinder position Y_C/S=1.0, two peaks are observed, which are much stronger than those in the two aforementioned cases. These strong peaks combined into one in the case where Y_C/S=1.5. Additionally, the positions of their peak values appear at the step for Y_C/S=1.0 and 1.5 when compared with the no-cylinder case and when Y_C/S=0.5. Fig. 7 presents the relationship between the time-spatially averaged Nusselt number and total pressure drop coefficient at various cross-stream positions. When compared with the no-cylinder case, a 114% overall heat transfer enhancement on the bottom wall is achieved by inserting a cylinder at Y_C/S=1.0, with a 45% increment in pressure drop. When Y_C/S=1.5, the heat transfer efficiency decreases, accompanied by an increasing pressure drop, when compared with that of Y_C/S=1.0. In conclusion, heat transfer is significantly enhanced when the cylinder position Y_C/S=1.0 along with a slight pressure drop.

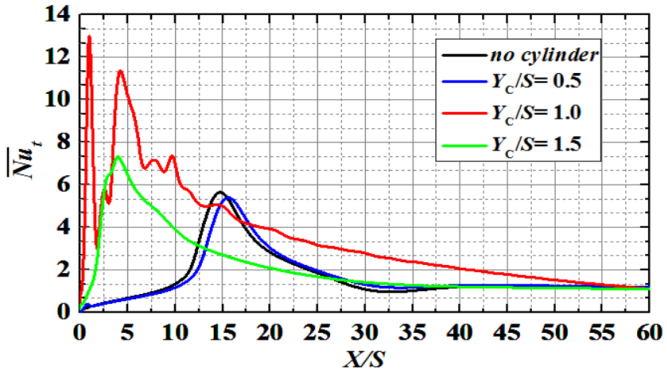

Figure 6. Time-averaged Nusselt number with various cross-stream positions for *Re* = 700.

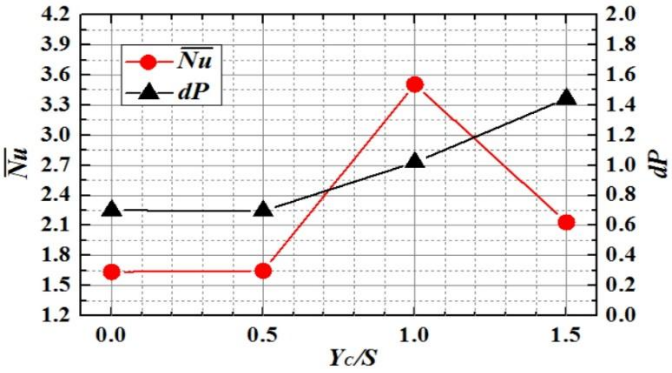

Figure 7. Time-spatially averaged Nusselt number and total pressure drop coefficient with various cross-stream positions for *Re* = 700.

B. Effect of the Streamwise Position

Considering cylinder position Y_C/S = 1.0, the flow patterns and heat transfer characteristics were investigated by changing the streamwise positions of the cylinder (X_C/S=0.6, 0.9, 1.2, 1.5). Time-averaged streamlines and streamwise velocity contours with various streamwise positions of a cylinder for *Re*=700 are shown in Fig. 8. The black arrows and red arrows in the figure represent the reattachment points of the primary and third recirculation zones, respectively. As the cylinder moves away from the step, the size of the primary recirculation zone and third recirculation zone increases, and their reattachment point moves downstream from the step. Contrarily, the size of the secondary recirculation zone along the upper wall decreases. When X_C/S=1.5, the secondary recirculation zone disappears while the fourth recirculation zone occurs along the bottom wall.

Fig. 9 shows the time-averaged Nusselt number distributions with various streamwise positions for *Re*=700. The peak positions of the time-averaged Nusselt number approximately correspond to the flow reattachment point of the primary and third recirculation zones. Thus, the peak positions move downstream of the step with the same variation trend of their reattachment points. The two peak values when X_C/S=0.9 are almost consistent with those when X_C/S=0.6. However, the two peak values decrease with an increase in the streamwise position from X_C/S=0.9 to X_C/S=1.5. As shown in Fig. 10, from X_C/S=0.6 to X_C/S=1.2, the heat transfer on the bottom wall slightly decreases with a slight increase in pressure drop. When X_C/S=1.5, the heat transfer performance significantly decreases. However, the heat transfer performance is the lowest in the case of no cylinder. Therefore, the cylinder is located at X_C/S=0.6, and when Y_C/S=1.0, the heat transfer performance is relatively optimum.

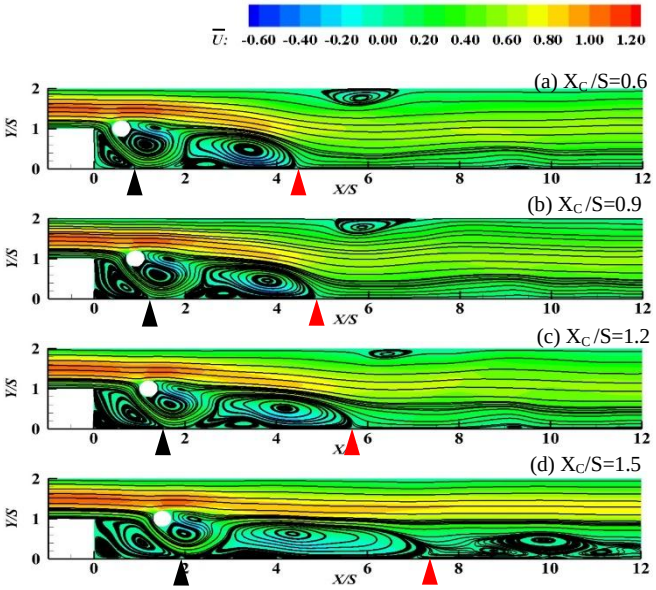

Figure 8. Time-averaged streamlines and streamwise velocity contours with various streamwise positions for *Re* = 700.

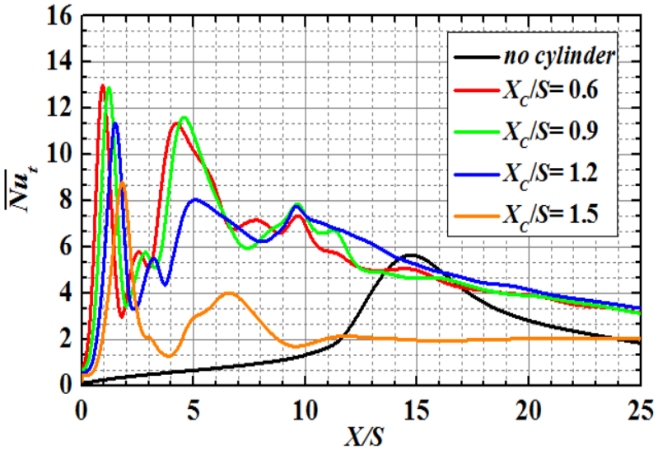

Figure 9. Time-averaged Nusselt number with various streamwise positions for *Re* = 700.

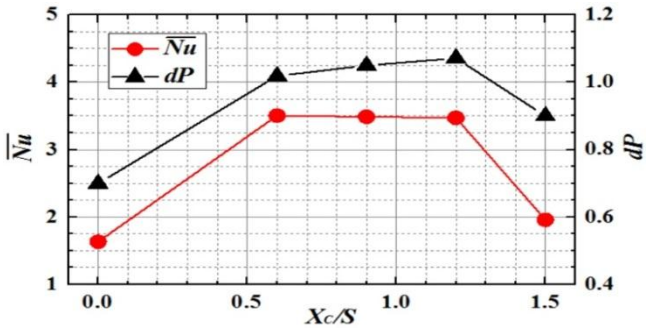

Figure 10. Time-spatially averaged Nusselt number and total pressure drop coefficient with various streamwise positions for *Re* = 700.

C. Heat Transfer Enhancement Mechanism

X_C/S=0.6 and Y_C/S=1.0 at *Re*=700 was selected to study the periodic flow instability and heat transfer enhancement mechanism in a transitional backward-facing step flow with an inserted cylinder. This selection was based on the results showing higher heat transfer and lower pressure drop described previously.

1) Periodic instability

Fig. 11 presents the monitor point results of the instantaneous transverse velocity (*V*) and power spectral density (*PSD*) of *V* at *Re*=700. Four monitor points P_1 (*X*/*S*=1.0, *Y*/*S*=1.0), P_2 (*X*/*S*=1.8, *Y*/*S*=1.0), P_3 (*X*/*S*=4.2, *Y*/*S*=1.0), and P_4 (*X*/*S*=6.6, *Y*/*S*=1.0) were set to monitor the *V* in the flow field. The fluid velocity fluctuates periodically with the frequency of the basic harmonic. The amplitude of the velocity oscillation increases gradually from point P_1 to P_3, but the amplitude of the velocity oscillation decreases at the downstream point P_4. At the upstream points P_1 and P_2, the power spectrum exhibits a single peak influenced by the inserted cylinder corresponding to the frequency f_C=14.11, while the power spectrum shows a secondary peak with f_S=7.25 at point P_4.

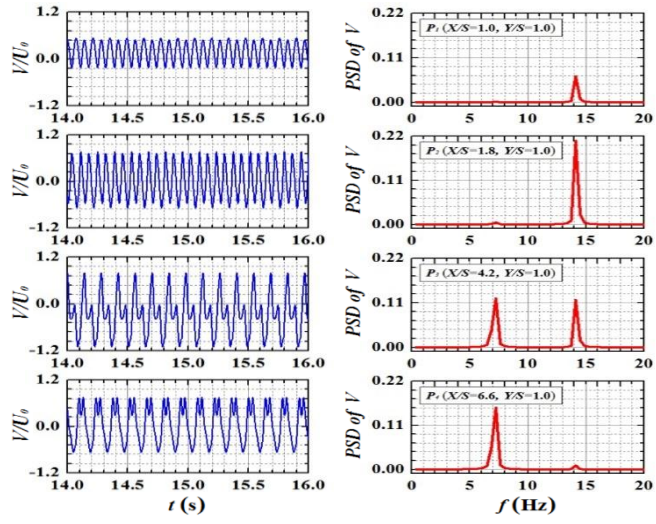

Figure 11. Monitor point results of transverse velocity (*V*) and power spectral density (*PSD*) of *V* at *Re* =700.

Thus, as the monitor point moves away from the cylinder, the periodic flow oscillation is primarily influenced by the channel, along with the lesser effect of the cylinder. Furthermore, at point P_3, the periodic velocity oscillation is dominated by two elementary frequencies (f_C and f_S) with the interaction of the cylinder and stepped channel. In Fig. 12, the time sequences of the instantaneous streamlines in one cycle are plotted. Vortexes A, B, and C are marked by green, red, and yellow arrows, respectively. Vortex B gradually becomes smaller and moves downstream of the step. In addition, as shown in Fig. 12(a)– (d), vortex A located behind the cylinder gradually sheds and combines with the smaller vortex attached to the bottom wall. As shown in Figs. 12(e)– (h), vortex C dissolves and combines with vortex A and the smaller vortex attaches to the bottom wall. This vortex motion explains the formation of vortex B, as shown in Fig. 12(a).

Fig. 13 shows the time sequences of the instantaneous vorticity contours combined with the instantaneous temperature contours in one cycle. The red parts correspond to the regions where the vorticity is positive, whereas the blue parts correspond to the regions where the vorticity is negative. Periodic development of the interaction between the positive and negative vorticity regions is essential in the thermal fields. Hence, the thermal boundary layer on the bottom wall deteriorates due to the effect of flow periodic instability.

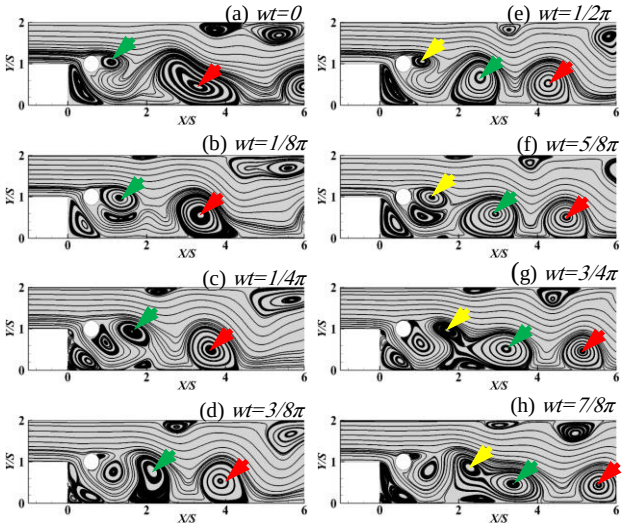

Figure 12. Time sequences of instantaneous streamlines in one cycle.

The instantaneous mappings of the fluctuating temperature contours superimposed with the fluctuating velocity vector are plotted in Fig. 14. Two fluctuating velocity components, *u* and *v*, and the fluctuating temperature θ are defined as follows:

$$u = \mathrm{U} - \overline{U} \tag{12}$$

$$\mathrm{v} = \mathrm{V} - \overline{\mathrm{V}} \tag{13}$$

$$\theta = \mathrm{T} - \overline{\mathrm{T}} \tag{14}$$

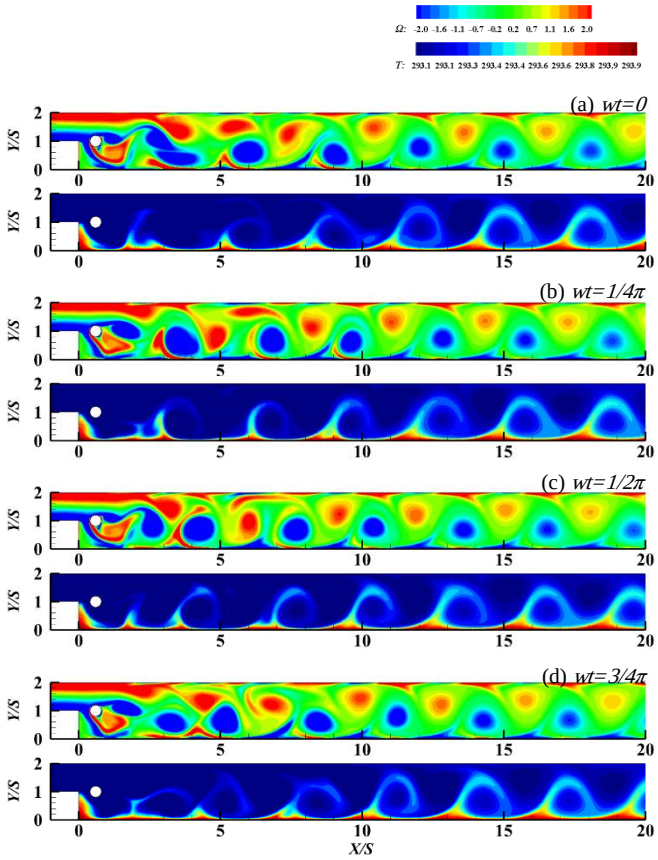

Figure 13. Instantaneous vorticity contours were combined with the instantaneous temperature contours in one cycle.

where $\overline{U}$ $\overline{V}$ correspond to the time-averaged streamwise velocity and normal components velocity, respectively, and $\overline{T}$ is the time-averaged temperature. From the qualitative analysis, Fig. 14 presents two types of fluctuating vortex motion corresponding to clockwise and counterclockwise directions of the vortices alternately. The red and blue parts represent the hot fluid ($\theta > 0$) and cold fluid ($\theta < 0$), respectively. The black and red arrows in the figure represent the positions of the peak and valley of the local *Nu*, respectively. Most peaks occur at the junction of hot and cold fluids, i.e., the heat transfer effect is better during the interaction. Irrespective of the type, the fluctuating vortex motion has positive effects on the heat transfer to the wall. This is due to the fluctuating vortex that necessitates the flow of the cold fluid from the main flow into the bottom wall. Contrarily, the fluctuating eddies pump away the hot fluid from the bottom wall. Furthermore, the mixing of the hot fluid and cold fluid with the effect of periodic instability of the flow leads to heat transfer enhancement on the bottom wall.

2) Statistical analysis

From the quantitative analysis, the monitor point P_5 (*X/S*=4.2, *Y/S*=0.02) near the position of the secondary peak of time-averaged *Nu* plotted in Fig. 6 is set to obtain the time sequences of fluctuating velocity (u, v) and fluctuating temperature (θ). Fig. 15 illustrates the time variation pattern of the fluctuating velocity field in ten cycles, which is assigned to four quadrants. The calculated fractional contributions to $-\overline{uv}$ and $\overline{v\theta}$ from each quadrant are shown in Table 3. Here, $-\overline{uv}$ represents the fluctuating velocity cross-correlation and $\overline{v\theta}$ represents the cross-correlation of the fluctuating velocity and temperature. As shown in Table 3, the number density of the plotted points is twice as large in the first quadrant ($u>0$, $v>0$) and third quadrant ($u<0$, $v<0$) when compared to those in the remaining two quadrants.

TABLE III. FRACTIONAL CONTRIBUTIONS TO $-\overline{uv}$ AND $\overline{v\theta}$ FROM EACH QUADRANT OF THE $U-V$ PLANE

Quadrant	Signs of u and v	Signs of θ	Number of data (n)	$\frac{\sum_{i=1}^{n}(uv)_i}{N\overline{uv}}$	$\frac{\sum_{i=1}^{n}(v\theta)_i}{N\overline{v\theta}}$
1	$u>0$	$\theta>0$	1602	1.076	0.479
	$v>0$	$\theta<0$	0	0	0
2	$u<0$	$\theta>0$	120	-0.056	0.013
	$v>0$	$\theta<0$	702	-0.812	-0.135
3	$u<0$	$\theta>0$	0	0	0
	$v<0$	$\theta<0$	1958	0.977	0.649
4	$u>0$	$\theta>0$	585	-0.178	-0.048
	$v<0$	$\theta<0$	309	-0.007	0.042

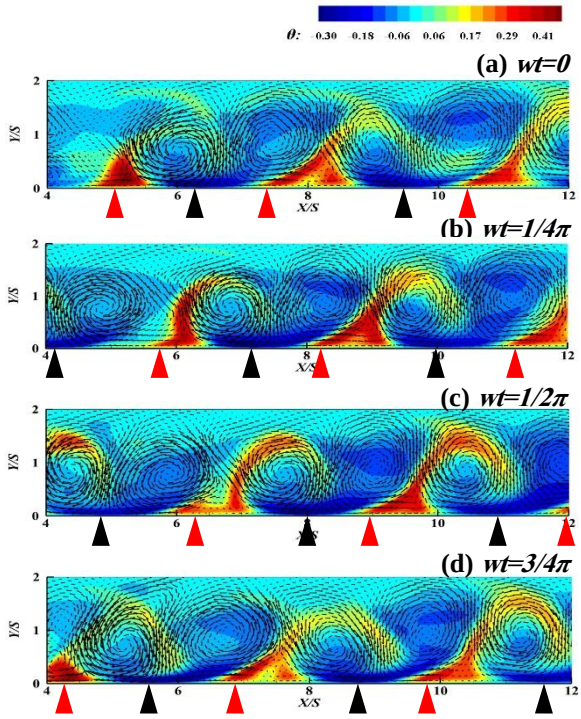

Figure 14. Instantaneous fluctuating velocity vector was combined with the instantaneous fluctuating temperature contours in one cycle.

The fractional contribution to $\overline{v\theta}$ from the hot fluid motion assigned to the first quadrant and from the cold fluid motion assigned to the third quadrant is much greater than that of the other types of fluid motions. Thus, pumping hot fluid from the bottom wall to the main flow region and entraining the cold fluid from the main flow region to the bottom wall region would result in the formation of the secondary peak of time-averaged Nu, as plotted in Fig. 6. Consequently, the heat transfer on the bottom wall is significantly enhanced when X_C/S=0.6 and Y_C/S=1.0.

IV. CONCLUSIONS

An incompressible numerical model for the backward-facing step with an inserted cylinder was established to investigate the effects of various streamwise and cross-stream positions of the cylinder on the flow fields and heat transfer. The following are the conclusions of the study:

- The simulation results in the case of no cylinder correspond well with the previously reported numerical and experimental results [4, 5, 30].
- The heat transfer of the transitional flow on the bottom wall is significantly enhanced when equipped with a cylinder located at X_C/S=0.6 and Y_C/S=1.0. The overall heat transfer enhancement on the bottom wall exhibited a 114% improvement in the presence of a cylinder and 45% increment in the pressure drop when compared with that of the case with no cylinder.
- Considering the effect of the periodic instability of the flow, the secondary peak of the time-averaged Nusselt number was observed when X_C/S=0.6 and Y_C/S=1.0. This occurred when the hot fluid was pumped from the bottom wall to the main flow region and the cold fluid was entrained from the main flow region to the proximal of the bottom wall.

ACKNOWLEDGMENT

The first author S. Zou gratefully acknowledges the financial support from China Scholarship Council (CSC) (No.201808320398), which has sponsored his Ph.D. study at the Doshisha University in Japan.

NOMENCLATURE

C_p	Specific heat capacity (J kg^{-1}K^{-1})
d	Diameter of the cylinder (m)
ER	Expansion ratio
f	Frequency (Hz)
h	Inlet channel height (m)
H	Outlet channel height (m)
k	Thermal conductivity (W m^{-1} K^{-1})
Nu	Local Nusselt number
$\overline{Nu_t}$	Time-averaged Nusselt number
$\overline{Nu}$	Time-spatial averaged Nusselt number
Pr	Prandtl number
P	Pressure (Pa)
q_W	Wall heat flux (W m^{-2})
Re	Reynolds number
S	Step height (m)
t	Time (s)
T	Temperature (K)
$\overline{T}$	Time-averaged temperature (K)
U_0	Averaged velocity component in the X direction (m s^{-1})
U	Streamwise velocity in the X direction (m s^{-1})
V	Transverse velocity in the Y direction (m s^{-1})
u	Streamwise fluctuating velocity (m s^{-1})
v	Transverse fluctuating velocity (m s^{-1})
$\overline{uv}$	Velocity cross-correction
$\overline{v\theta}$	Velocity-temperature cross-correction
W	Channel width (m)
X	Streamwise coordinate (m)
Y	Transverse coordinate (m)
X_C	Stream-wise position of the cylinder (m)
Y_C	Cross-stream position of the cylinder (m)
X_R	Time-averaged reattachment length (m)

Greek letters

Ω	Instantaneous vorticity (s^{-1})
θ	Fluctuating temperature (K)
μ	Dynamic viscosity (kg m^{-1} s^{-1})
ρ	Density (kg m^{-3})
τ	Sampling time (s)

Subscripts

max	Maximum
min	Minimum
0	Inlet value
out	Outlet value
W	Wall value

REFERENCES

[1] A. S. Kherbeet *et al.*, "Heat transfer and fluid flow over microscale backward and forward facing step: a review," *International Communications in Heat and Mass Transfer*, vol. 76, pp. 237-244, 2016.

[2] H. Abu-Mulaweh, "A review of research on laminar mixed convection flow over backward-and forward-facing steps," *International Journal of Thermal Sciences*, vol. 42, no. 9, pp. 897-909, 2003.

[3] H. Togun, "Effect of laminar separation flow and nanofluids on heat transfer augmentation with passive techniques: A review," *International Communications in Heat and Mass Transfer*, vol. 77, pp. 9-14, 2016.

[4] B. F. Armaly, F. Durst, J. Pereira, and B. Schönung, "Experimental and theoretical investigation of backward-facing step flow," *Journal of fluid Mechanics*, vol. 127, pp. 473-496, 1983.

[5] T. Lee and D. Mateescu, "Experimental and numerical investigation of 2-D backward-facing step flow," *Journal of Fluids and Structures*, vol. 12, no. 6, pp. 703-716, 1998.

[6] P. Kapiris and D. Mathioulakis, "Experimental study of vortical structures in a periodically perturbed flow over a backward-facing step," *International journal of heat and fluid flow*, vol. 47, pp. 101-112, 2014.

[7] S. Terhaar, A. Velazquez, J. Arias, and M. Sanchez-Sanz, "Experimental study on the unsteady laminar heat transfer downstream of a backwards facing step," *International communications in heat and mass transfer*, vol. 37, no. 5, pp. 457-462, 2010.

[8] B. Armaly, A. Li, and J. Nie, "Three-dimensional forced convection flow adjacent to backward-facing step," *Journal of thermophysics and heat transfer*, vol. 16, no. 2, pp. 222-227, 2002.

[9] H. Barrios-Pina, S. Viazzo, and C. Rey, "A numerical study of laminar and transitional mixed convection flow over a backward-facing step," *Computers & fluids*, vol. 56, pp. 77-91, 2012.

[10] G. Biswas, M. Breuer, and F. Durst, "Backward-facing step flows for various expansion ratios at low and moderate Reynolds numbers," *J. Fluids Eng.*, vol. 126, no. 3, pp. 362-374, 2004.

[11] Y. Chen, J. Nie, H.-T. Hsieh, and L. Sun, "Three-dimensional convection flow adjacent to inclined backward-facing step," *International Journal of Heat and Mass Transfer*, vol. 49, no. 25-26, pp. 4795-4803, 2006.

[12] J. Nie and B. F. Armaly, "Three-dimensional convective flow adjacent to backward-facing step-effects of step height," *International journal of heat and mass transfer*, vol. 45, no. 12, pp. 2431-2438, 2002.

[13] J. H. Nie, Y. Chen, and H.-T. Hsieh, "Effects of a baffle on separated convection flow adjacent to backward-facing step," *International Journal of Thermal Sciences*, vol. 48, no. 3, pp. 618-625, 2009.

[14] J. Nie and B. F. Armaly, "Reattachment of three-dimensional flow adjacent to backward-facing step," *J. Heat Transfer*, vol. 125, no. 3, pp. 422-428, 2003.

[15] T. Chiang and T. W. Sheu, "A numerical revisit of backward-facing step flow problem," *Physics of fluids*, vol. 11, no. 4, pp. 862-874, 1999.

[16] H. Iwai, K. Nakabe, and K. Suzuki, "Flow and heat transfer characteristics of backward-facing step laminar flow in a rectangular duct," *International journal of heat and mass transfer*, vol. 43, no. 3, pp. 457-471, 2000.

[17] H. Lan, B. Armaly, and J. Drallmeier, "Three-dimensional simulation of turbulent forced convection in a duct with backward-facing step," *International journal of heat and mass transfer*, vol. 52, no. 7-8, pp. 1690-1700, 2009.

[18] L. Kaiktsis, G. E. Karniadakis, and S. A. Orszag, "Onset of three-dimensionality, equilibria, and early transition in flow over a backward-facing step," *Journal of Fluid Mechanics*, vol. 231, pp. 501-528, 1991.

[19] F. Schäfer, M. Breuer, and F. Durst, "The dynamics of the transitional flow over a backward-facing step," *Journal of Fluid Mechanics*, vol. 623, pp. 85-119, 2009.

[20] A. Kitoh, K. Sugawara, H. Yoshikawa, and T. Ota, "Expansion ratio effects on three-dimensional separated flow and heat transfer around backward-facing steps," 2007.

[21] J. Xu, S. Zou, K. Inaoka, and G. Xi, "Effect of Reynolds number on flow and heat transfer in incompressible forced convection over a 3D backward-facing step," *International Journal of Refrigeration*, vol. 79, pp. 164-175, 2017.

[22] J. Tihon, V. Pěnkavová, J. Havlica, and M. Šimčík, "The transitional backward-facing step flow in a water channel with variable expansion geometry," *Experimental Thermal and Fluid Science*, vol. 40, pp. 112-125, 2012.

[23] A. Kumar and A. K. Dhiman, "Effect of a circular cylinder on separated forced convection at a backward-facing step," *International journal of thermal sciences*, vol. 52, pp. 176-185, 2012.

[24] F. Selimefendigil and H. F. Öztop, "Identification of forced convection in pulsating flow at a backward facing step with a stationary cylinder subjected to nanofluid," *International Communications in Heat and Mass Transfer*, vol. 45, pp. 111-121, 2013.

[25] H. Mohammed, O. A. Alawi, and M. Wahid, "Mixed convective nanofluid flow in a channel having backward-facing step with a baffle," *Powder Technology*, vol. 275, pp. 329-343, 2015.

[26] F. Selimefendigil and H. F. Öztop, "Forced convection and thermal predictions of pulsating nanofluid flow over a backward facing step with a corrugated bottom wall," *International Journal of Heat and Mass Transfer*, vol. 110, pp. 231-247, 2017.

[27] R. K. Shah and A. L. London, *Laminar flow forced convection in ducts: a source book for compact heat exchanger analytical data*. New York: Academic press, 2014, p. 3.

[28] S. V. Patankar and D. B. Spalding, "A calculation procedure for heat, mass and momentum transfer in three-dimensional parabolic flows," in *Numerical prediction of flow, heat transfer, turbulence and combustion*: Elsevier, 1983, pp. 54-73.

[29] J. P. Guerrero and R. Cotta, "Benchmark integral transform results for flow over a backward-facing step," *Computers & fluids*, vol. 25, no. 5, pp. 527-540, 1996.

[30] K. Sugawara, E. Kaihara, H. Yoshikawa, and T. Ota, "DNS of Three-Dimensional Unsteady Separated Flow and Heat Transfer Around a Downward Step," in *ASME 2005 Summer Heat Transfer Conference collocated with the ASME 2005 Pacific Rim Technical Conference and Exhibition on Integration and Packaging of MEMS, NEMS, and Electronic Systems*, 2005: American Society of Mechanical Engineers Digital Collection, pp. 469-477.

How to Cite this Article:

Zou, S., Xu, J. H., Inaoka, K. & Xi, G. N. (2020). Transitional Flow and Heat Transfer over a Backward-Facing Step with an Inserted Cylinder. International Journal of Science and Engineering Investigations (IJSEI), 9(102), 59-67. http://www.ijsei.com/papers/ijsei-910220-08.pdf